Seismic Attributes Application for the Distributed Acoustic Sensing Data for the Marcellus Shale: New Insights to Cross-Stage Flow Communication

Payam Kavousi Ghahfarokhi, Timothy Carr, and Liaosha Song, West Virginia University; Priyavrat Shukla and Piyush Pankaj, Schlumberger

Abstract

Recently, oil and gas companies started to invest in fiber optic technology to remotely monitor subsurface response to stimulation. Distributed Acoustic Sensing (DAS) and Distributed Temperature Sensing (DTS) record vibration and temperature around the fiber, respectively. In this research, we introduce new seismic attributes calculated from the DAS data that could suggest cross-stage fluid communication during hydraulic fracturing. The DAS data covers the entire 28 stimulated stages of the lateral MIP-3H well close to Morgantown, WV. We calculated the energy attribute for the DAS data of the studied stages. Subsequently, a Hilbert transform is applied to the DAS data to evaluate the instantaneous frequency of each trace in the DAS. In addition, we applied a fast Fourier transform to each trace for all the SEGY files to calculate the dominant frequency with a 30 second temporal window. The dominant frequency is compared to the DTS data and energy attribute for the stages in the horizontal MIP-3H well. The DTS analysis shows that stimulation of the stages 10 causes a temperature rise in the previous stage 9; in contrast, stage 18 stimulation does not affect stage 17 temperature. We suggest that the common low frequency zone identified in instantaneous frequency and dominant frequency attributes between stages 10 and 9 is related to presence of fluid and gas that transferred cross-stage during hydraulic fracturing. The fluid and results in the frequency damping of the vibrations around the fiber. We show that the frequency attribute reveals increases detail about the stimulation than conventional signal energy attribute of the DAS data.

Introduction

The multidisciplinary and multi-institutional team at Marcellus Shale Energy and Environmental Laboratory (MSEEL) work on geoscience, engineering, and environmental research in collaboration with Northeast Natural Energy LLC., several industrial partners, and the National Energy Technology Laboratory of the US Department of Energy. The purpose of this unique research is to develop and test new knowledge and technology to improve recovery efficiency, while diminishing environmental implications of unconventional resource development. Before 2015, the two horizontal wells MIP-4H and MIP-6H were producing gas from the Marcellus Shale near Morgantown, West Virginia (Figure 1). Two other horizontal wells MIP-3H and MIP-5H were completed in 2015. Fiber optics technology including distributed acoustic

sensing (DAS) and distributed temperature sensing (DTS), were deployed in the MIP-3H horizontal well near Morgantown, West Virginia to provide continuous subsurface vibration and temperature sampling during stimulation. The MIP-3H stimulation over 28 stages involved injection, at high pressure, averaging 8500 psi (58.6 MPa), to break the formation and establish a complex network of permeable fracture pathways.
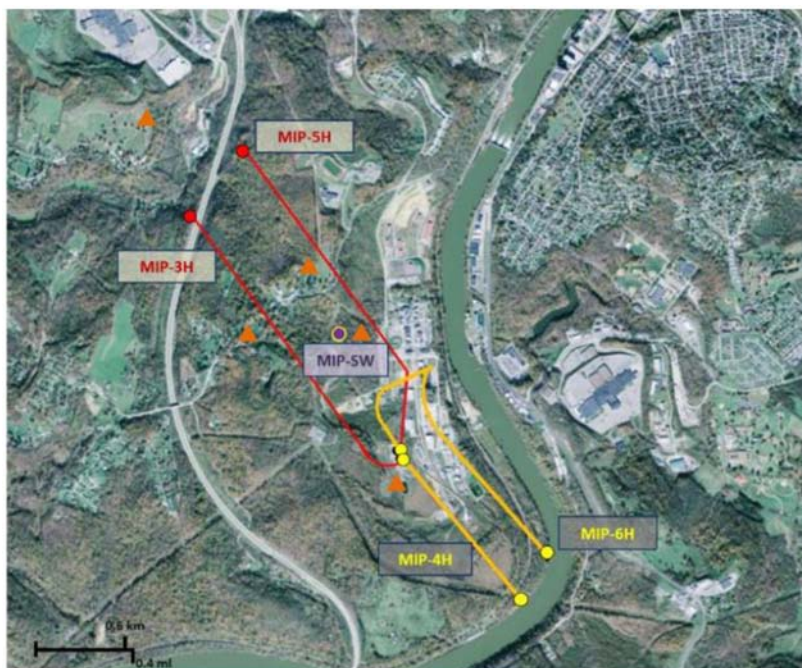
Figure 1—Marcellus Shale Energy and Environment Laboratory (MSEEL) just outside Morgantown, West Virginia, USA. The MSEEL site consists of four horizontal production wells operated by Northeast Natural Energy LLC. (MIP-3H, MIP-4H, MIP-5H, MIP-6H), two pilot holes (MIP-3 and MIP-4), a micro-seismic and sampled observation well (MIP-SW), and a grid of five surface seismometer (triangles).

The first well in the Marcellus shale was completed in October 2004. In 2005, all horizontal wells drilled in Pennsylvania were conventional wells. Since the end of 2008 there was a surge in horizontal well drilling activity in the Marcellus shale, which peaked in 2013 and 2014 (Beckwith, 2013), and with that came widespread multi-stage hydraulic fracturing. During hydraulic fracturing, large quantities of fluids are pumped to create the fracture followed by proppant to hold the fracture open. With time, operators have evolved their completion designs and pumped bigger job sizes to improve production performance. Average lateral lengths increased from 4,000 ft. to 6,000 ft. and proppant volumes more than doubled between 2010 to 2014 (Kugler et al., 2015). The fracture connects to the matrix and provides a large surface area and conductive pathway for fluids to flow from matrix to the wellbore. Therefore, more than fracture conductivity, matrix deliverability plays a critical role in production from unconventional reservoirs (Economides et al., 2000). Uncontrollable factors like geology and reservoir quality also play a dominant role in the success of a well. Neural network models developed on 48 Marcellus wells concluded that gas production is proportional to depth, thickness and hydrocarbon maturity (Shelley et al., 2014). However, controllable factors like completion quality play an important role. Operators have used engineered completion designs, which place perforation clusters in similarly stressed areas to achieve uniform stimulation along the wellbore. Such completions have increased the EUR in Marcellus shale wells by 30% in some cases (Walker et al., 2012). Researchers have also analyzed channel fracs, a technique to create highly conductive fractures, and its applicability to Marcellus shale (Ajayi et al., 2011).

Natural fracture presence plays an important role in the production performance of shale wells by creating a complex fracture network during hydraulic fracturing. Outcrop analysis, image logs, caliper logs, regional

stress trends and seismic ant tracking are methods used in mapping natural fractures. Stochastic methods are commonly used to create a distribution of natural fractures based on their intensity. During the fracturing operation, natural fractures can also lead to cross stage communication, which can be sensed using fiber optic technology as discussed in this paper. The ultimate success of hydraulic fracturing is known only by the production results, but diagnostic methods help to understand the performance of a fracturing job in real time.

Traditionally, surface pressure and subsurface pressure gauges, well head rates, and radioactive tracers are the only monitoring tool for completion engineers during the hydraulic fracturing (Mollennar et al., 2012). Shallow depth of investigation limits the application of the traditional techniques in complex reservoirs (Mollennar et al., 2012). The need for more robust diagnostic tools encouraged the oil and gas companies to use fiber-optic technology. Fiber-optic sensing technology has been applied to the oil and gas reservoirs from 1990s to monitor steam injection, injection profiling, acid injection profiling, and hydraulic fracture diagnostics (Karaman et al., 1996; Rahman et al., 2011; Glasbergen et al., 2010; Sierra et al., 2008; Holly and Kalia, 2015). The early application of the fiber-optic technology was Distributed Temperature Sensing (DTS), which was only able to record the temperature. DTS is still widely used for unconventional oil and gas reservoir to monitor the temperature in the subsurface during stimulation, production, or injection. Distributed acoustic sensing (DAS) technology was later introduced to the industry to perform more robust diagnostics of the subsurface (Molenaar et al., 2012). It was originally developed in the defense industry, and has become popular in the oil and gas industry with application from completion to production to abandonment. DAS or distributed vibration sensing (DVS) uses optical fibers to measure the dynamic strain at all points along the fiber (Parker et al., 2014). These remote sensing techniques have provided unparalleled acoustic sampling from the subsurface during hydraulic fracturing. When the fiber-optic technology is employed, a single silica fiber with protective jacket is clamped to the outer part of the production casing (Figure 2).
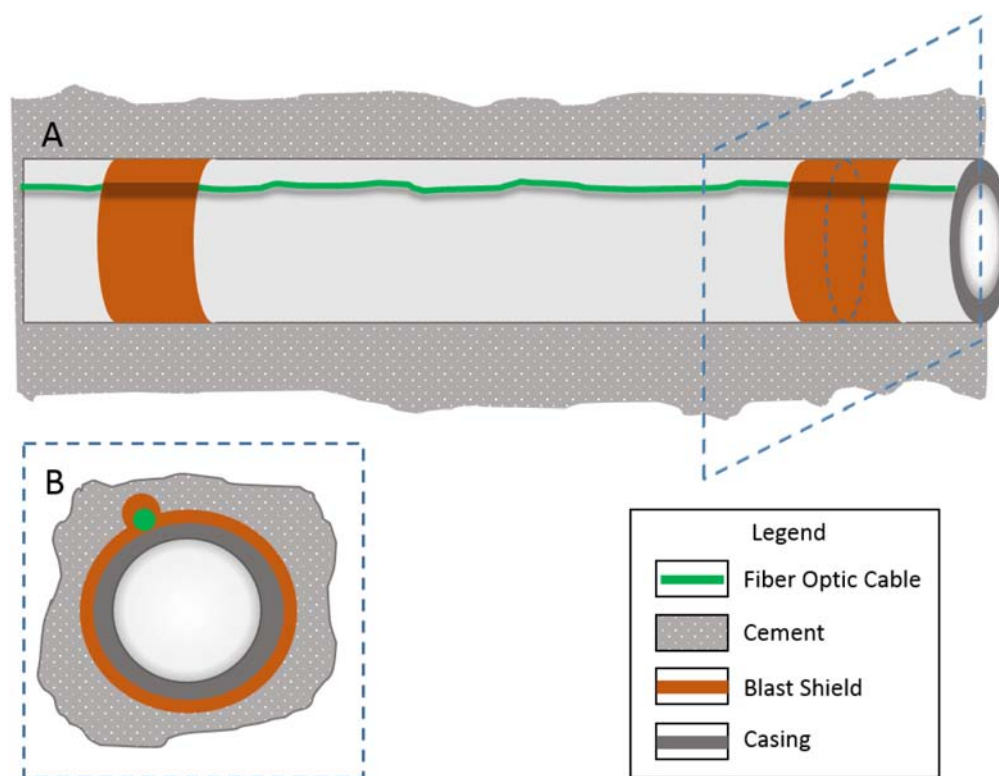
Figure 2—Schematic depiction of the fiber-optic-cable installation. (A), the cable is attached to the outer part of the production casing and surrounded by the cement, notice the cable is not straight. (B), profile view of cable installation. The location of the profile is illustrated in (A) with dash lines. Image is not to scale.

This permanent in-well fiber brings the possibility of time-lapsed measurements and monitoring without well intervention and production deferment. The first field application of DAS was undertaken by Shell Canada during the completion of a tight gas well in February 2009 to optimize the treatment (Mestayer et al., 2011; Molenaar et al., 2012). The DAS technology has also been utilized for the Vertical Seismic Profiling (VSP) as a replacement for geophones (Miller et al., 2012; Bakku et al., 2014; Mateeva et al.,2012; Mateeva et al., 2013; Madsen et al., 2013). Webster et al., (2013) used DAS to detect microseismic events and verified their results with geophones in the borehole.

DAS technology has provided a near real-time tool for hydraulic fracturing monitoring without well intervention (Mollennar et al., 2012; Mollennar and Cox, 2013; Bakku et al, 2014; MacPhail et al., 2012). Unlike traditional hydraulic fracturing monitoring techniques that require movement of the acquisition system for each stage stimulation, DAS uses a fiber that can be permanently attached to the production casing. Thus, it removes the time delay of several hours and facilitates decision making for completion engineers.

Boone et al., (2015) showed that DAS can be used to characterize perforating gun signature to measure the zero timing of the perf detonation down to microseconds. For cemented plug and perf (CPnP) completions, an optimal hydraulic fracturing depends on proper seating of plug and the ball on it to isolate the perforated casing from the completion below. The ball seating on the plug generates a strong signature on the DAS (Boone et al., 2015).

The DAS senses the vibration in the local environment around the fiber and provides a measure of the relative strain of the optical fiber. The technology is based on the optical time domain reflectometry (OTDR). OTDR systems include a laser light transmitter and an optical detector. High power laser transmitter sends an accurately timed light down the sensing fiber; because of impurities inherent in the glass core, the lights are scattered back to the detector. A tiny fraction (<0.000001%) of the forward propagating pulse backscatters toward the detector as the pulse travels through the fiber. Measuring the power and the wavelength of the backscattered light enables the detector to estimate the temperature, strain, or the vibro-acoustic on the fiber (Tanimola and Hill, 2009). Any incident angle above the critical angle results in light refraction and hence dissipation in the surroundings.

The time delay and the amplitude of the backscattered wave is used by the OTDR detector to calculate the point at which backscattering has occurred. A fiber optic can be envisioned as a series of tiny mirrors joined together; any movement of these mirrors modify the backscattered waves, which can be measured (Kimble, 2013). Changes of physical environment around the fiber such as temperature, dynamic strain, and vibro-acoustic disturbance alter the mirror's reflective characteristics (Kimble, 2013). The sensitivity of the fiber to the vibro-acoustic waves around it will convert the entire fiber to an array of microphones that can detect vibrations around the fiber. The DAS data is usually processed as series of hearing devices using a gauge length parameter (Figure 3). The DAS detector unit (interrogation unit) sends consecutive light pulses into the fiber, the backscattered signal of the first pulse are S1 and S2; the second emitted pulse get backscattered as S1' and S2' from the beginning and end of the gauge length, respectively (Figure 3). By measuring the phase lag between the backscattered signals from the two end-points of the gauge lengths, the relative strain can be relatively estimated (Li et al., 2015). The backscattered pulse can be processed every 100μsec corresponding to a 10 kHz sampling rate. Parameters can be adjusted to optimize the performance of the operation (Mollennar and Cox, 2013). DAS continuously processes the phase lags of the backscattered. However, simultaneous processing of backscattered is limited to 40,960 sensing points. This limitation brings the receiver spacing between 1 to 10 meters (Conway and Mondanos, 2015).
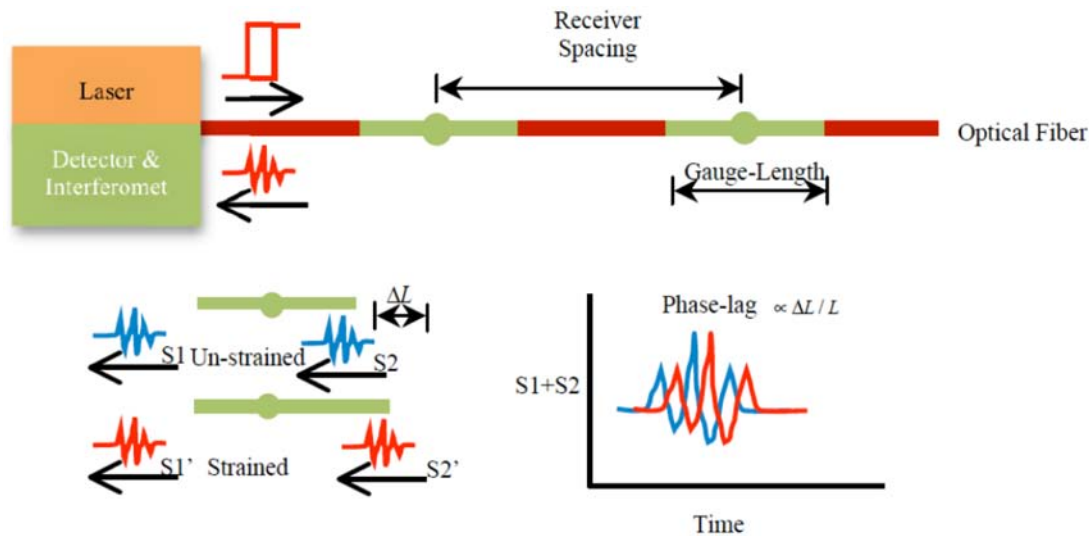
Figure 3—DAS measurements principle. (S1+S2) represents the sum of the backscattered signals from the front and the end of the gauge length in un-strained fiber for the first emitted pulse. (S1'+S2') is the sum of the backscattered signals of the second emitted pulse. The backscattered signals are from the front and the end of the gauge length after the fiber is deformed. The phase lag between (S1+S2) and (S1'+S2') is proportional to the fiber stain. Courtesy of Li et al., (2015).

The distributed temperature sensing (DTS) data can also be recorded from the same fiber deployed in the well. The temperature can be estimated from the backscattered light spectrum. DTS technology measures the "Stokes" and "Anti-Stokes" components of the backscattered spectrum (Figure 4). The "Anti-Stokes" component is sensitive to the temperature, while the stoke component is temperature independent. Thus, a ratio of "Anti-Stokes" and "Stoke" power provides a measure for the temperature (Molenaar et al., 2012).
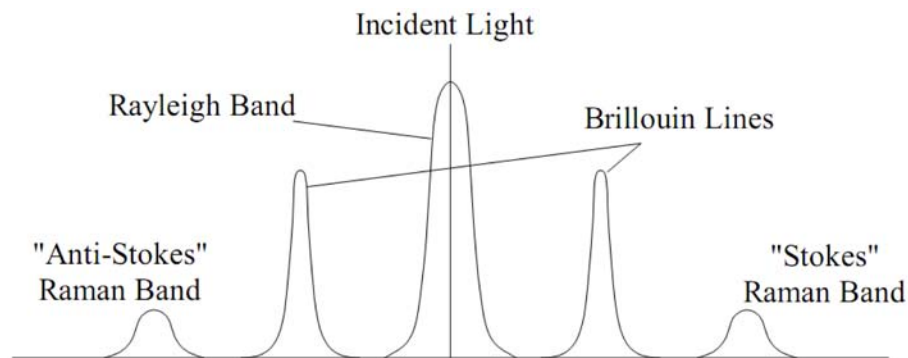
Figure 4—The backscatted light spectrum has Rayleigh Band, Brillouin bans, and Raman bands. Rayleigh band are sensitive to strain while Raman band are sensitive to the temperature around the fiber (courtesy Carnahan et al.,1999)

Geologic background

The Marcellus Shale spans 95,000 square miles (246,000km^2) across six states in northeastern U.S., which makes it the most extensive shale-gas play in North America (Carr et al., 2011; Wang and Carr, 2013). Marcellus Shale is in the lower portion of Hamilton Group, middle Devonian, and it is overlain by Tully Limestone and Mahantango Formation. Cherry Valley Limestone divides the upper and lower Marcellus Shale (Figure 5). The Marcellus Shale is a distal marine mudstone within a westward-prograding foreland succession deposited in the Appalachian basin, which represents a periodically deepening basin tied to tectonics during the Acadian orogeny (Ettensohn, 1985; Lash and Engelder, 2011, Zagorski et al., 2012; Carr et al., 2013; Milliken et al., 2013; Song et al., 2017). Dominant marine medium-gray to gray burrowed mudstone interbedded with silty mudstone, siltstone, and sandstone intervals are interpreted to reflect regional shallowing, and finely laminated, dark gray to black, organic-rich mudstone, commonly associated

with thin beds of skeletal carbonate are interpreted to reflect relative deepening (Ettensohn, 1985; Ettensohn et al., 1988). Ettensohn 1985 and Ettensohn et al., 1988 ascribe these deepening events to a tectono-stratigraphic model. However, Sageman et al., 2003 presented an oscillating seasonal dysoxia – anoxia model, and argued that relative sea-level, a combination of tectonic subsidence and eustasy, is the controlling factor. The Marcellus Shale has recently attracted attention as an important gas-producing unit (Engelder and Lash, 2008; Zagorski et al., 2012). The paleogeography from the Middle Devonian shows that Well MIP-3H is located in the middle of the basin (Figure 6). The lateral of the MIP-3H is drilled just above the Cherry Valley Limestone in the Upper Marcellus Shale (Figure 7).
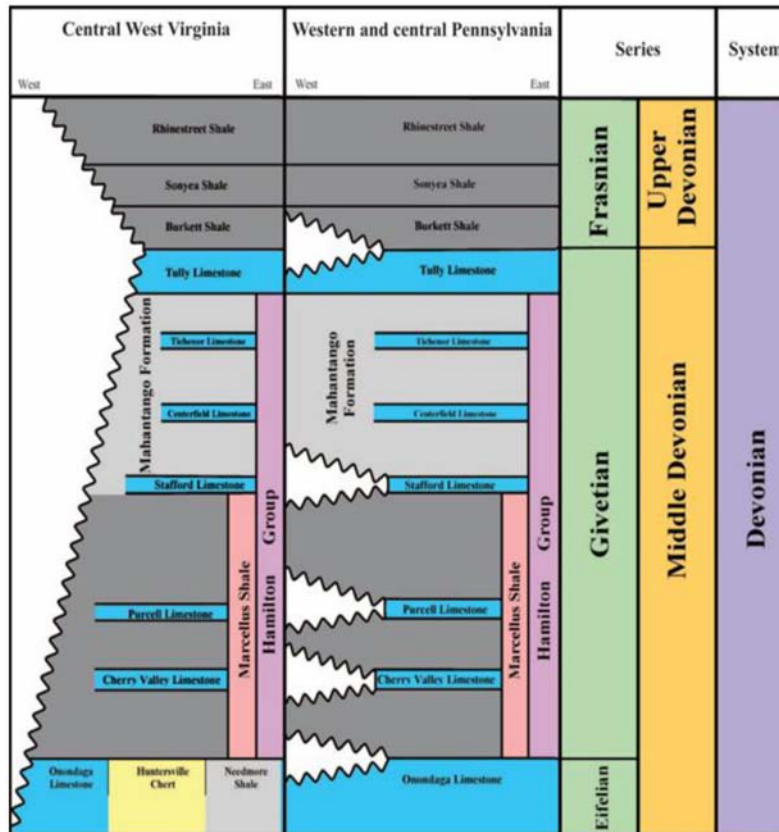
Figure 5—Middle Devonian stratigraphy in West Virginia and Pennsylvania (from Zagorski et al., 2012).

Figure 6—Reconstruction of Middle Devonian paleogeography (from Blakey, 2010). The study well (MIP-3H) is in the middle of the basin.
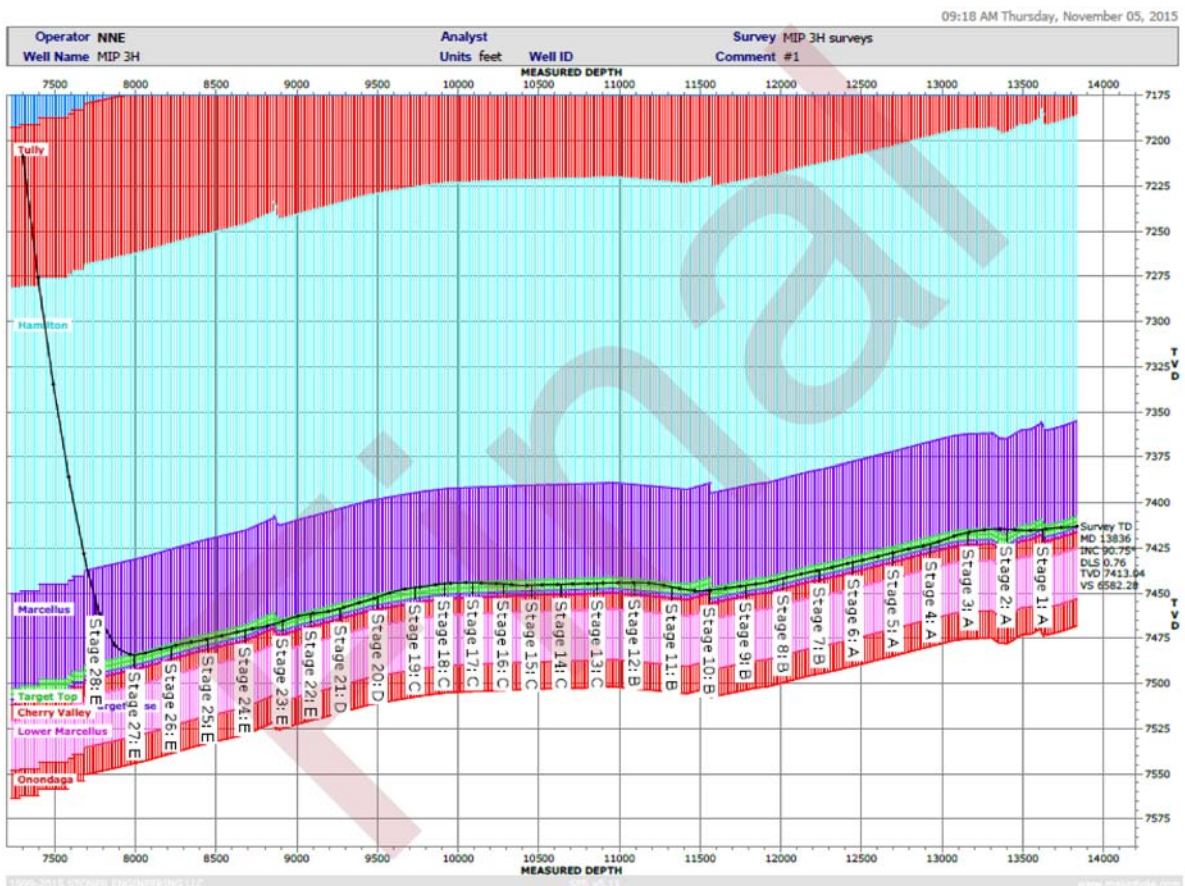
Figure 7—The MIP-3H lateral was kept above the Cherry Valley Limestone in the Upper Marcellus Shale.

Methodology

The DAS data are in binary format and recorded as SEGY files for every 30 seconds of the stimulation job. The SEGY file is comprised of 493 traces and 200 to 300 SEGY files that typically encompass a moderate sized 2-3 hours stimulation. The DAS data covers the entire 28 stages of the lateral MIP-3H. Figure 8 shows a single 30 seconds SEGY file recorded during the stimulation of the stage 14 of MIP-3H well. The SEGY file has 493 traces with 60,000 samples per trace. This is equivalent to sampling rate of 0.5 msec. Seismic attributes are widely used to extract information; such as frequency, amplitude, attenuation, etc. from seismic traces. We show that these attributes can also be employed for distributed acoustic sensing data to extract more subtle information than common energy attribute about the hydraulic fracturing process, especially the cross-stage flow communications.
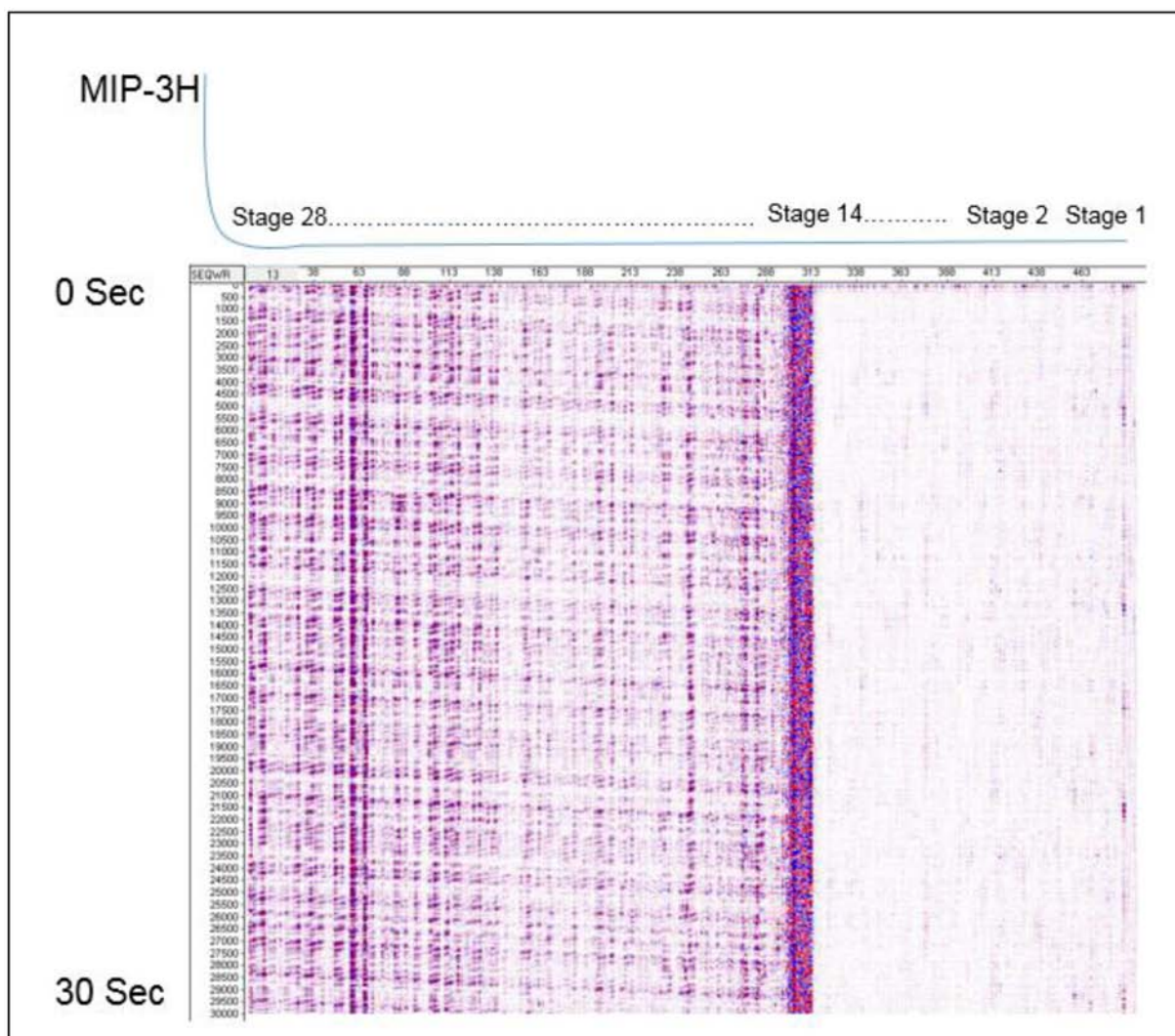
Figure 8—A single 30 seconds SEGY file recorded during the stimulation of the stage 14 of MIP-3H well. Minimal vibrations are recorded for stage 1 to stage 13 because these stages were separated from stage 14 to stage 28 by a plug.

We applied several common seismic attributes to the DAS data. These attributes include energy, instantaneous attributes, and dominant frequency. The computations are conveyed through an in-house processing software developed in the MSEEL research group at West Virginia University.

Energy Attribute
The energy of a discrete signal can be calculated as:

$$E = \sum_{n=-\infty}^{\infty} |x(n)|^2 . \tag{Eq. 1}$$

Each SEGY file has 493 traces and 60,000 samples. We calculate an energy attribute with a 30 seconds temporal window. The energy attribute for a SEGY file can be calculated as (Kavousi et al., 2017):

$$E_{ik} = \sum_{j=1}^{60,000} x_k(j)^2 \quad i = 1 \dots 493, k = 1 \dots Number\ of\ the\ SEGY\ files. \tag{Eq. 2}$$

Where $x_k(j)$ is sample j from 60,000 samples in trace i from k^{th} SEGY file. Thus, there are 493 energy values calculated for every time step of 30 seconds during the fracture stimulation for each SEGY file.

Instantaneous attributes

A seismic trace can be assumed as a projection of an analytic signal (complex signal) on the real domain. Attributes such as instantaneous frequency, instantaneous phase, and instantaneous amplitude can be calculated at any sample of the trace using the analytic complex signal. Complex traces were introduced to reflection seismology in early 70's and later followed by instantaneous attribute traces for seismic analysis (White, 1991). A complex trace separates phase from amplitude and then allows calculation of instantaneous attributes (Zhang and Bentley, 2000). Complex trace analysis has been applied to geophysical data processing by Barnes (1990, 1991, 1992 and 1993), Bodine (1984), Farnbach (1975), Ha et al., (1991), Robertson et al., (1984 and 1988), Taner et al., (1977 and 1979) and White (1991). The instantaneous attributes are available through most of the seismic interpretation workstations. These attributes describe the waveform shape of the seismic trace. The two basic instantaneous attributes are instantaneous amplitude and instantaneous phase. Instantaneous frequency is the differential of instantaneous phase. The analytic signal can be assumed as a spring, the more contracted the spring, the higher the instantaneous frequencies (Figure 9). The imaginary part of the analytic signal is called quadrature trace, which can be found by a 90° phase shift to the real signal. A peak or a trough in the real signal corresponds to a zero-crossing in the imaginary signal, and vice versa. The imaginary signal can be calculate using a Hilbert transform.
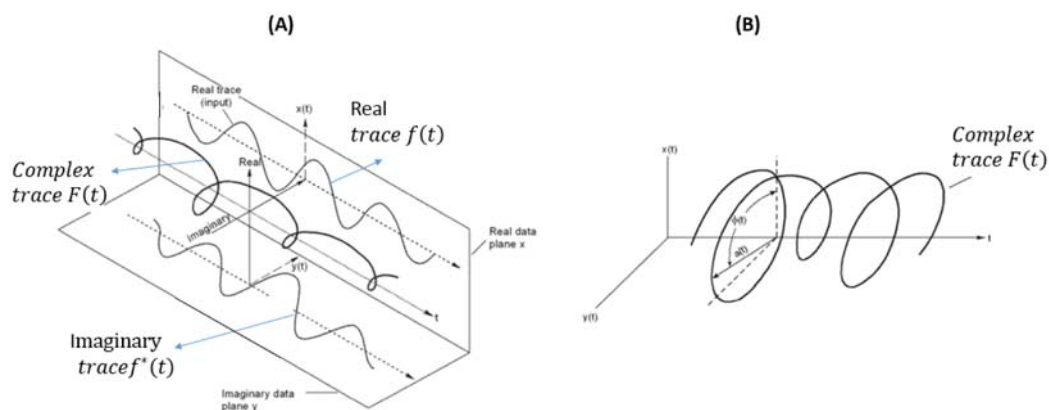
Figure 9—(A) The real trace is the projection of the complex trace on the real plane. The imaginary trace is the Hilbert transform of the real Trace. (B) The a(t) is the vector perpendicular to the time axis which connects it to the complex trace, its length is referred as the instantaneous amplitude at time t. θ(t), the instantaneous phase, is the angle that vector a(t) makes with the vertical axis at time (t) (Modified from Hardage, 2010).

Seismic data transformation is often used to extract information about the waveform that are not visible in the real domain amplitude-time data. One of the most common transformation of time series is the Fourier transform, which takes time series (seismic data) to the frequency domain. Fourier transform allows

the evaluation of the frequency content of a portion of seismic trace; however, it does not provide local measurement of the frequency for example at single sample in the seismic trace (Taner et al., 1977). Other transformation such as Hilbert transform can be used to calculate the analytic (complex) signal for instantaneous amplitude and instantaneous phase evaluations. The latter two attributes are the basis for evaluating instantaneous frequency at each sample of the seismic trace. Complex signal calculation for the seismic data was introduced by Taner et al., (1977). A seismic trace $f(t)$ can be considered as the real part of a complex trace (Figure 9):

$$F(t) = f(t) + if^*(t), \qquad \text{(Eq. 3)}$$

where $f^*(t)$ is the imaginary signal (quadrature signal) calculated by a 90° phase shift of the real signal using a Hilbert transform. The real trace $f(t)$ can be expressed as a time-dependent amplitude $A(t)$ and a time dependent phase $\theta(t)$ as (Taner, 1977):

$$f(t) = A(t) \cos \theta(t). \qquad \text{(Eq. 4)}$$

The quadrature signal then has a 90° phase shift relative to the real trace:

$$f^*(t) = A(t) \sin \theta(t), \qquad \text{(Eq. 5)}$$

and the complex trace is:

$$F(t) = f(t) + jf^*(t) = A(t)e^{i\theta(t)}. \qquad \text{(Eq. 6)}$$

Knowing the $f^*(t)$ and $f(t)$, we can find $A(t)$ and $\theta(t)$:

$$A(t) = \sqrt{f^2(t) + f^{*2}(t)} = |F(t)|, \qquad \text{(Eq. 7)}$$

and

$$\theta(t) = \tan^{-1}[f^*(t)/f(t)]. \qquad \text{(Eq. 8)}$$

$A(t)$ and $\theta(t)$ are instantaneous amplitude (trace envelope) and instantaneous phase of the complex trace, respectively. Then, the instantaneous frequency can be calculated as the derivative of the instantaneous phase:

$$\omega(t) = \frac{d}{d(t)}\{\tan^{-1}[f^*(t)/f(t)]\} = \frac{f(t)\frac{df^*(t)}{dt} + f^*(t)\frac{df(t)}{dt}}{f^2(t) + f^{*2}(t)}. \qquad \text{(Eq. 9)}$$

The empirical observations suggested that there is a shift toward low frequency zones below gas sands (Taner, 1977). Rocks that are saturated with oil and gas cause the high frequency attenuation. Tai (2009) undertook a time-frequency analysis and showed that gas saturated sands are associated with low frequency zones. One possible explanation would be the damping effect of the gas sands that filters out the higher frequencies. We propose the similar idea for the distributed acoustic sensing (DAS) data; when the fiber is surrounded by higher saturation of fluid/gas, its vibration is dampened relatively fast and high frequencies are attenuated. Thus, the spectrum of the DAS signals shifts toward lower frequencies. As an analogy, a spring that is oscillating in a viscous fluid dies faster (i.e. higher frequency oscillations get attenuated faster) than a spring oscillating in the air. This phenomenon is referred as an "overdamped" oscillation in the engineering literatures (Alciatore, 2007; Rao and Qiu, 1993).

Dominant Frequency

Fourier transform shows the similarity between various frequencies sinusoids and the seismic trace (Barnes, 1998). Frequency analysis deals with frequency contents of each on dimension (1D) trace at the time domain. It transforms each 1D signal into the frequency domain by means of frequency decomposition algorithms such as fast Fourier transform. For length N input trace x, the discrete Fourier transform (DFT) is a length N trace X, with elements:

$$X(k) = \sum_{n=1}^{N} x(n)e^{\left(\frac{-2\pi i(k-1)(n-1)}{N}\right)} \qquad 1 \leq k \leq N.$$

(Eq. 10)

Frequency analysis has been extensively carried out to find time varying spectral properties of seismic data (Barnes, 1993). Three parameters are usually used to characterize a frequency spectra: the center frequency, the spectral bandwidth, and the dominant frequency (Widess, 1982; Kallweit and Wood, 1982; Berkhout, 1984). The average frequency of the power spectrum is referred as central frequency, and the standard deviation around the central frequency is defined as the spectral bandwidth (Figure 10) (Berkhout, 1984). The dominant frequency is the density of amplitude maxima in the power spectrum (Kallweit and Wood, 1982; Widess, 1982; Yilmaz, 1987; Sheriff, 1995). The second moment of the power spectrum is also equivalent to the dominant frequency (Barnes, 1993).
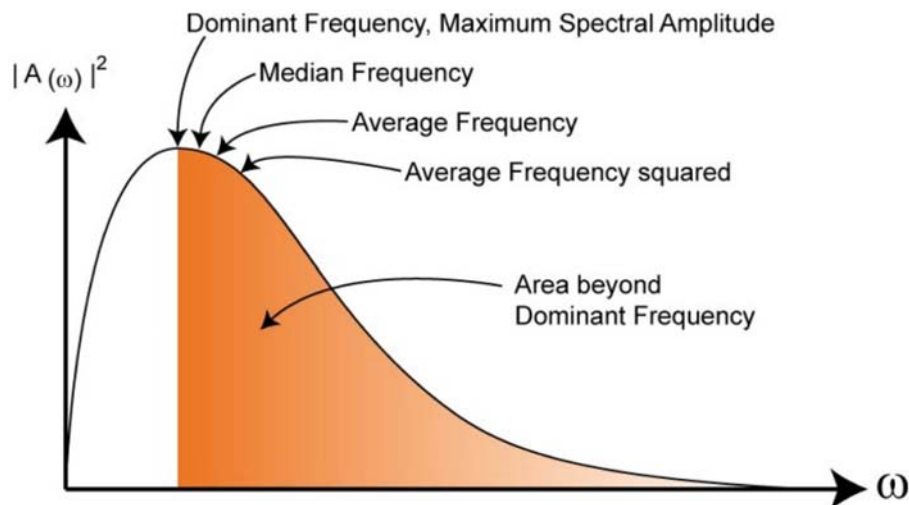
Figure 10—The frequency attributes that can be calculated from the spectrum resulted from Eq.10 (OpendTect Documentation).

We applied a fast Fourier transform to each trace for all the 220 SEGY files to calculate the dominant frequency with a 30 seconds temporal window. The dominant frequency is compared to the DTS data and energy attribute for stage 10 and stage 18 stimulation in the MIP-3H well. We propose that damping effect is also detectable in dominant frequency attribute. Higher frequencies are attenuated when the fiber is surrounded by the gassy fluid. Hence, low dominant frequency zones are evident.

Results and Discussions

We calculated the energy, instantaneous frequency, and dominant frequency attributes for several stimulated stages in MIP-3H lateral. One common way to visualize the DAS data is to use a waterfall plot; it has the measured depth of the well in the vertical axis and number of the timesteps in the horizontal axis. The color shows the calculated attribute for that timestep.

Figure 11 is the calculated energy attribute for stage18 in MIP-3H. 220 SEGY files form 220 timesteps of 30 seconds for 493 traces. Usually the visualization window will be limited to the zone of the interest around the stimulated stage (Figure 11).
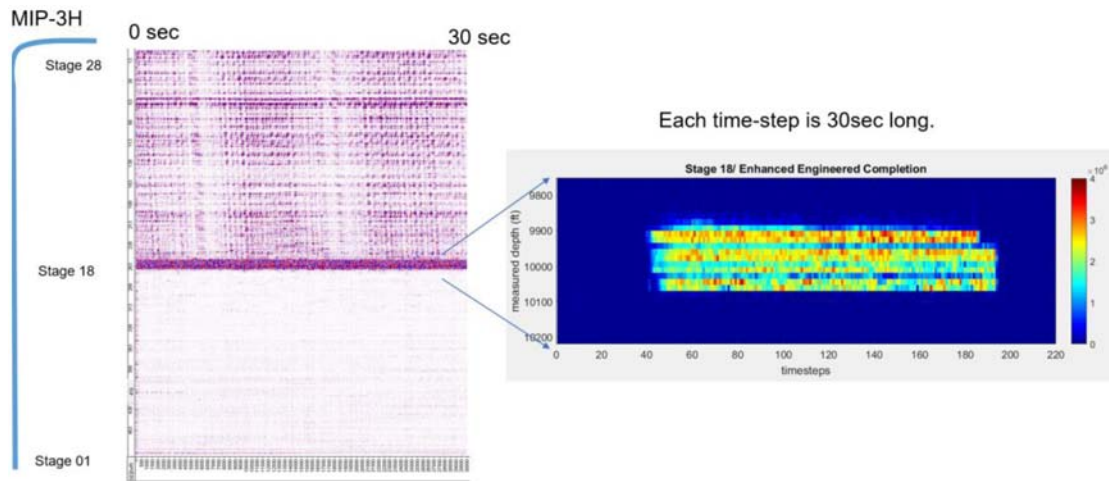
Figure 11—The energy attribute is evaluated for the stage 18 in MIP-3H well. The Eq.2 is used to calculate the energy attribute for the traces in vicinity of the stage 18 for 220 SEGY files (i.e. 110 minutes stimulation job).

In this study, we focus on stage 10 attribute analysis. The instantaneous frequency and the amplitude of the DAS data are calculated for every 0.5 millisecond (Sampling rate of the DAS data). Figure 12 shows local low frequency zones in stage 9 during stage 10 stimulation. DAS amplitude does not reveal significant energy for stage 9. The plug and perf mechanism is employed for the completion of the MIP-3H. This procedure seals the direct connections between stage 10 and stage 9 through the wellbore. Stimulation of the stage 9 took place around 2 hours before stage 10 stimulation. The fracturing fluid of stage 9 rested at the formation and got warmed to almost the reservoir temperature of 160 °F. Subsequent stimulation of stage 10 pushed the warmed gassy fluid of stage 9 back toward the well through fractures and faults and hence a temperature rise is observed in the DTS data. High fracture intensity close to the base of the stage 10 and top of the stage 9 are observed in the wireline image logs (Figure 12).
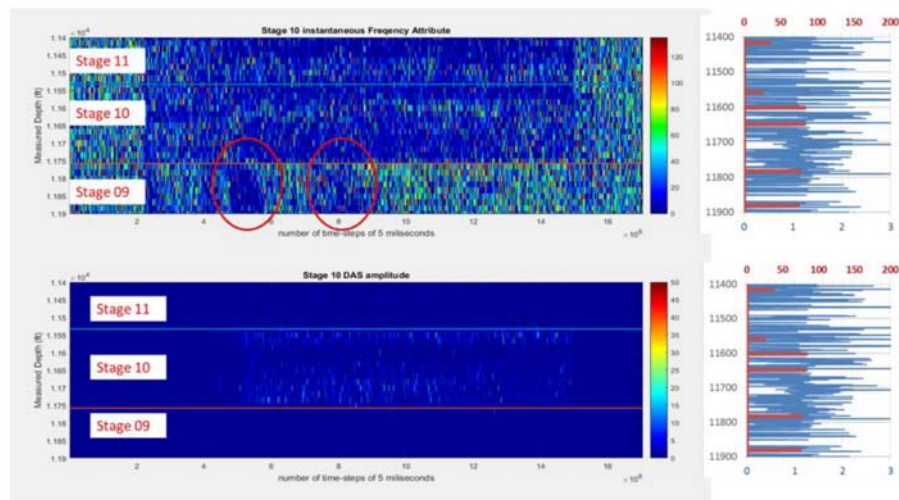
Figure 12—Instantaneous frequency shows that the stimulation of the stage 10 results in low frequency zones in stage 9 while the vibration amplitude does not reveal any vibration. The blue bars in the histograms on the right of the waterfall plots show the fracture intensity at each depth.

In addition to the DAS data, the DTS data are also recorded during the stage 10 stimulation. DTS shows that the temperature increases in stage 9 while fracturing stage 10 (Figure 13). Amini et al., 2017 and Carr et al., 2017 noticed this temperature rise for several other stages in MIP-3H. They suggested that numerous fractures and faults close to the stage boundaries are possibly responsible for this abnormal observation.
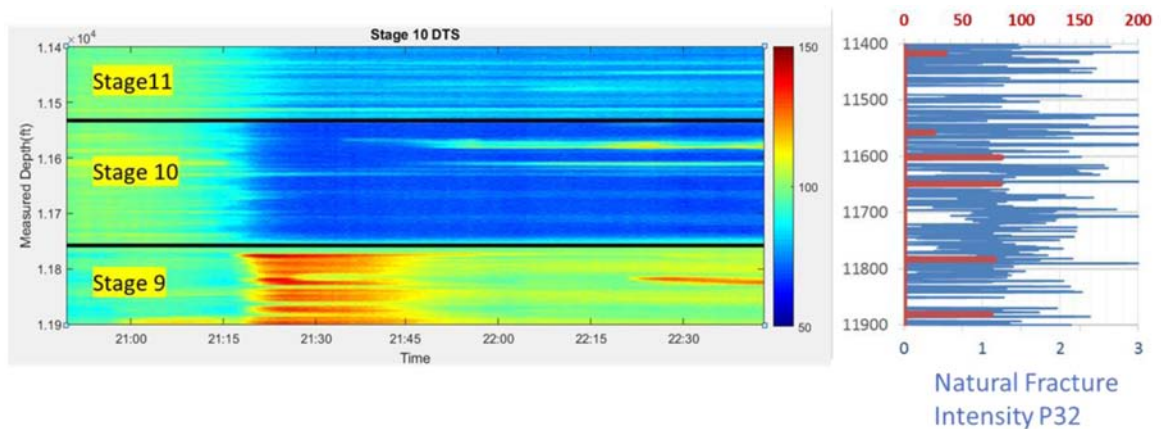
Figure 13—The stage 10 stimulation increased the stage 9 temperature.
Note the high fracture intensity at the upper part of the stage 9.

Wilson et al., (2016) studied the natural fractures in the MIP-3H lateral and MIP-3H pilot well (the vertical well) and extracted the trends of the natural fractures. A single fracture set oriented in N79°E was observed in the MIP-3H. The image logs from the vertical MIP-3H Pilot showed two set of fractures: an open fracture set oriented in N57°E and a healed fracture set in N87°E (Figure 14).
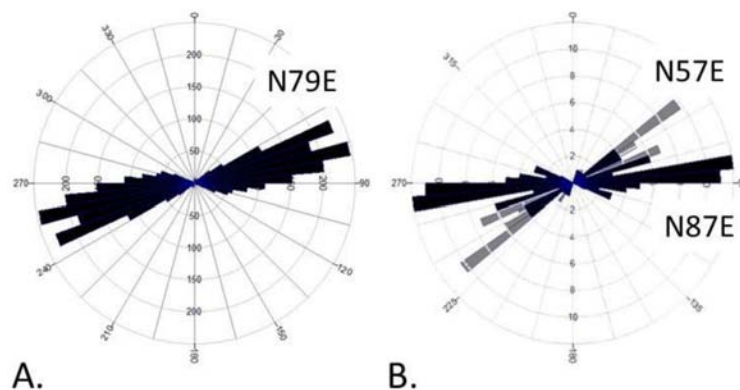
Figure 14—Rose diagrams of natural fractures a) observed along the length of the MIP-3H lateral
(N=1640) and B) in the vertical pilot well (N=91). Fractures observed in the vertical well consist of 21
open fractures (light grey color) in the N57°E cluster and 70 healed fractures mainly concentrated in
the N87°E cluster with a smaller fraction falling in the N57°E cluster. (Courtesy of Wilson et al.,2017)

Carr et al., (2017) used the interpreted orientation of fractures in both MIP-3H and MIP-3H Pilot and proposed a conceptual model to explain the temperature rise in stage 9, during stimulation of the stage 10 (Figure 15). The conceptual model has two pre-existing natural fracture sets oriented at N79°E and N57°E. MIP-3H is oriented in N36°W; hence, hydraulic fractures could form along non-critically oriented N79°E preexisting fractures in the lower Marcellus Shale as aseismic "slow slip" they were detected at surface stations but not detected by standard microseismic monitoring (Figure 1) (Kumar et al. 2016). The oblique orientation of the lateral well to the preexisting fractures could explain the warming as detected by DTS of stage 9 to near formation temperatures by movement of fluids previously injected and warmed by the formation through stimulated fractures communicating from stage 10 to stage 9.
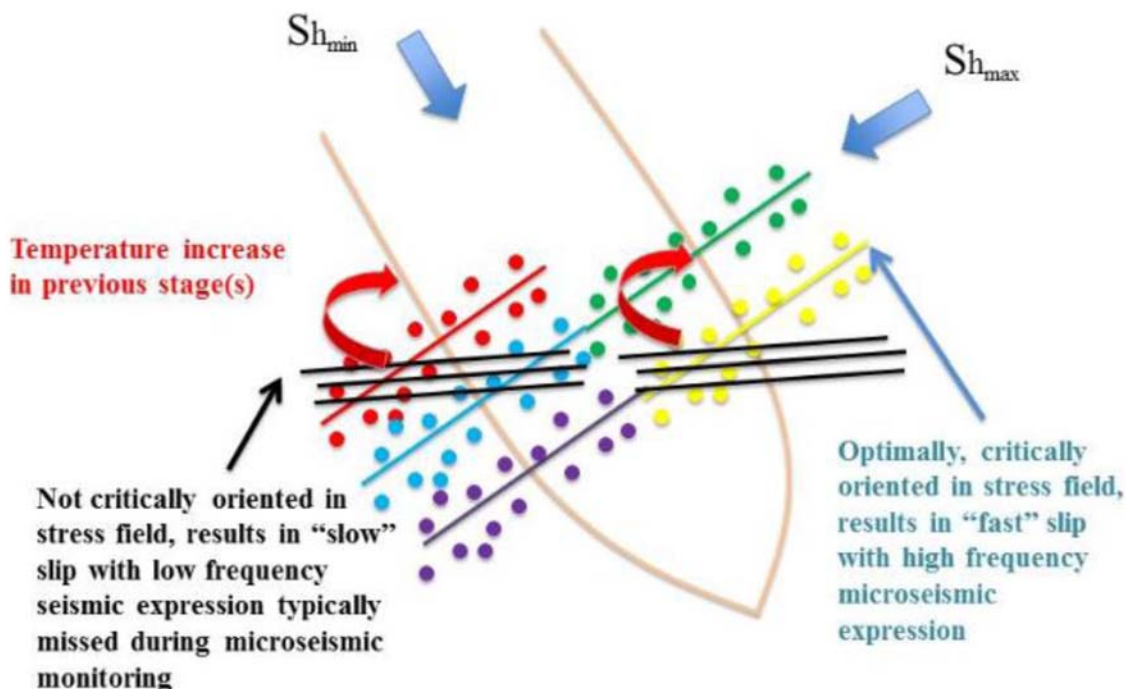
Figure 15—Conceptual model of observed pattern of the numerous preexisting N87°E fractures and faults observed in logs, microseismic orientated N59°E, LPLD events and warming observed in DTS in previous stages during fracture stimulation in the MIP-3H. Basic figure was modified from Das and Zoback, 2012. Movement and injection along non-critically oriented preexisting fractures in the lower Marcellus Shale resulted in the "slow" slip with low frequency seismic expression that was not picked up by microseismic monitoring and movement of fluids warmed by the formation to previous stimulated stages. Microseismic events follow optimal oriented fractures to the present-day stress regime and are centered significantly above the stimulated interval. The observed microseismic events may be the expression of the stress on overlying layers imposed by the injection of more than 250 cubic feet of sand and fluid per foot of lateral.

Subsequently, we evaluated the proposed attributes to see the relationship between frequency content, energy attribute, and the temperature rise for the stage 10. Figure 16 shows that the temperature rise is associated with low dominant frequency and instantaneous frequency in stage 9 during stimulation of stage 10. We suggest that a frequency damping effect is happening around the fiber due to the back-circulating of the gassy fluid toward the well. The fiber vibration is affected by the gassy fluid presence and higher frequency vibrations are dampened. It results in low frequency zone in stage 9, which also shows abnormal temperature. Neither the energy attribute nor the instantaneous amplitude attribute show these abnormal zones associated with high temperature. One more explanation could be the fractures (both natural fractures and tensile fractures from stage 9 stimulation) dampen the vibrations. As an analogy, a highly fractured rock vibrates in lower frequencies than a pristine piece of rock. However, this explanation cannot justify high frequency zones in stage 9. If it was only fractures responsible for the low frequencies, there would be low frequency zones for the entire stimulation job (Figure 16). There might be contribution from both fluid and fractures in dampening the high frequencies.
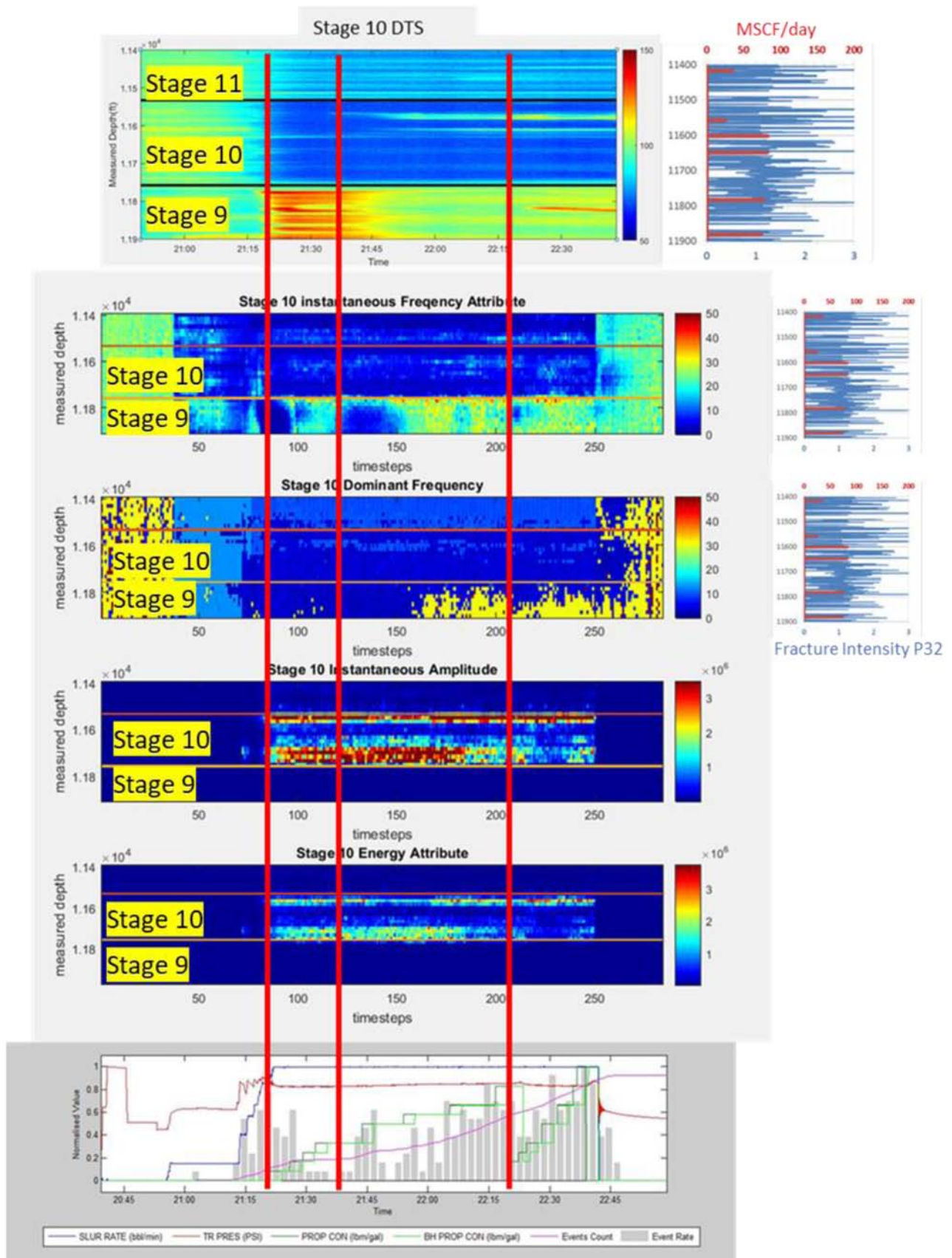
Figure 16—DTS data and stimulation parameters are compared with energy, instantaneous frequency, instantaneous amplitude, and dominant frequency. Low frequency zones are observed when there is a temperature rise in stage 9. Note that the proppant drop also creates low frequency zones in stage 9.

We also notice that there is frequency drop when there is proppant concentration drop, this might be due to the proppants that hinder the fluid flow communication between the stages. A drop in the proppant concentration entails more hydraulic connections between the two stages, an abnormal temperature rise and a frequency attenuation. On the other hand, stage 18 stimulation does not significantly raise the temperature or create a low frequency zone in stage 17 (Figure 17). Wireline image logs show less fracture intensity at the base of the stage 18 and top of the stage 17 than base of the stage 10 and top of the stage 9, respectively.
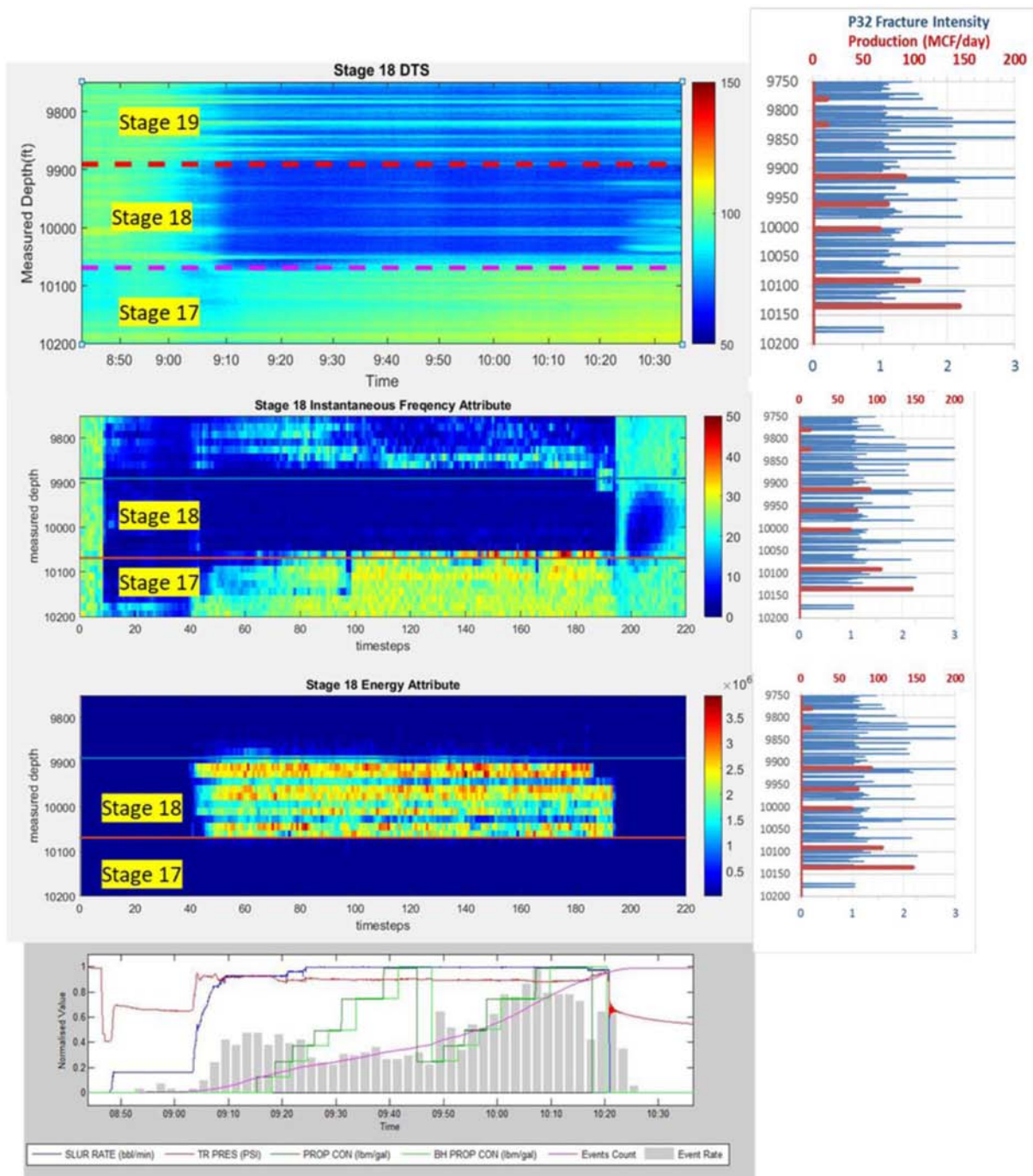
Figure 17—DTS data and stimulation parameters are compared with energy, instantaneous frequency, instantaneous amplitude, and dominant frequency. Neither the temperature rise nor the low frequency zones are significant in stage17 while stage 18 Stimulation.

Conclusions

1. Frequency attribute has been shown to be a valuable tool to extract subtle spectrum variations of the DAS signals.
2. Instantaneous frequency can be calculated for each of the 60,000 samples of 493 traces in every SEGY file. However, this computation requires a considerably powerful workstation for 200-300 SEGY files for each stage; in addition, the waterfall plot for 835,000,000 samples is not very easy to understand. Our results show that a temporal window of 30 seconds would make the calculations faster and generates a smoother image to visualize.
3. Although energy attribute calculation is computationally cheaper than frequency attributes, it does not show any abnormal energy variations in stage 9 while stimulation of the stage 10.
4. The temperature rise was attributed to the hydraulic connection between the stage 9 and stage 10. This connection is probably intensified by natural fractures oriented obliquely to the lateral in the reservoir.
5. Stage 18 stimulation does not cause a temperature rise in the stage 17. Instantaneous frequency also does not show a significant frequency drop in DAS response for the stage 17. This behavior is attributed to the low natural fracture intensity P32 at the base and top of the stage 18 and 17, respectively.
6. We also noticed low frequency zone in stage 9 when the proppant concentration was dropped during stage 10 stimulation. One possible explanation could be that high proppant concentration hinders the fluid communications between stage 9 and 10.
7. The less critically oriented N81°E natural fractures in the stress field seem to intensify the cross-stage flow communications. These fractures undergo slow slip and did not show significant microseismic expressions. However, more than 1500 of these fractures were observed in the wireline image logs.

Future Work

One might try an adaptive moving temporal window that has variable size in different locations of the DAS traces. For example, the smaller window size could be utilized near the top and bottom of the stimulated stages to catch more details of the frequency spectrum while a larger window could be employed for places in the middle of the stimulated stages. Other seismic attributes can be tested for the fiber optic data. The similarity attribute would be a proposed attribute to be tested for traces around the boundary of the stimulated stages.

Acknowledgements

References

Ajayi, B. T., Walker, K. J., Wutherich, K., & Sink, J. (2011, January 1). Channel Hydraulic Fracturing and Its Applicability in the Marcellus Shale. *Society of Petroleum Engineers*. doi: 10.2118/149426-MS.

Alciatore, D.G., 2007. *Introduction to mechatronics and measurement systems*. Tata McGraw-Hill Education.

Amini, S., Kavousi, P. and Carr, T.R., 2017. Application of Fiber-optic Temperature Data Analysis in Hydraulic Fracturing Evaluation--A Case Study in Marcellus Shale. Unconventional Resources Technology Conference (URTEC).

Bakku, S.K., Fehler, M. and Wills, P., 2014. Monitoring hydraulic fracturing using distributed acoustic sensing in a treatment well. In *SEG Technical Program Expanded Abstracts 2014* (pp. 5003-5008). Society of Exploration Geophysicists.

Barnes, A.E., 1990. Analysis of temporal variations in average frequency and amplitude of COCORP deep seismic reflection data. In *SEG Technical Program Expanded Abstracts 1990* (pp. 1553-1556). Society of Exploration Geophysicists.

Barnes, A.E., 1991. Instantaneous frequency and amplitude at the envelope peak of a constant-phase wavelet. *Geophysics*, **56**(7), pp.1058-1060.

Barnes, A.E., 1992. Another look at NMO stretch. *Geophysics*, **57**(5), pp.749-751.

Barnes, A.E., 1993. Instantaneous spectral bandwidth and dominant frequency with applications to seismic reflection data. *Geophysics*, **58**(3), pp.419-428.

Barnes, A.E., 1998. The complex seismic trace made simple. *The Leading Edge*, **17**(4), pp.473-473.

Beckwith, R. (2013, June 1). The Marcellus Shale Gas Boom Evolves. *Society of Petroleum Engineers*. doi: 10.2118/0613-0034-JPT.

Berkout, A.J., 1984. Seismic resolution: Resolving power of acoustical echo techniques. *Handbook of Geophysical Exploration, Section I, Seismic Exploration*, Geophysical Press, London, pp.181-192.

Bodine, J.H., 1984. Waveform analysis with seismic attributes. In *SEG Technical Program Expanded Abstracts 1984* (pp. 505-509). Society of Exploration Geophysicists.

Boone*, K., Crickmore, R., Werdeg, Z., Laing, C. and Molenaar, M., 2015, July. Monitoring hydraulic fracturing operations using fiber-optic distributed acoustic sensing. In Unconventional Resources Technology Conference, San Antonio, Texas, 20-22 July 2015 (pp. 316-322). Society of Exploration Geophysicists, American Association of Petroleum Geologists, Society of Petroleum Engineers.

Carr, T.R., Wilson, T.H., Kavousi, P., Amini, S., Sharma, S., Hewitt, J., Costello, I., Carney, B.J., Jordon, E., Yates, M. and MacPhail, K., 2017. Insights from the Marcellus Shale Energy and Environment Laboratory (MSEEL). Unconventional Resources Technology Conference (URTEC).

Carr, T.R., Wang, G., Boyce, M.L. and Yanni, A., 2011, March. Understanding controls on deposition of organic content in the Middle Devonian organic-rich shale intervals of West Virginia and western Pennsylvania. In Geological Society of America Abstracts with Programs: Northeast (46th Annual) and North-Central (45th Annual) Joint Meeting, Pittsburgh (Vol. **43**, No. 1, p. 50).

Carr, T.R., Wang, G. and McClain, T., 2013, March. Petrophysical analysis and sequence stratigraphy of the Utica shale and Marcellus shale, Appalachian Basin, USA. In IPTC 2013: International Petroleum Technology Conference.

Carnahan, B.D., Clanton, R.W., Koehler, K.D., Harkins, G.O. and Williams, G.R., 1999, January. Fiber Optic Temperature Monitoring Technology. In *SPE Western Regional Meeting*. *Society of Petroleum Engineers*.

Conway, C. and Mondanos, M., 2015, June. An introduction to fibre optic Intelligent Distributed Acoustic Sensing (iDAS) technology for power industry applications. In Proceedings of the 9th International Conference on Insulated Power Cables, Versailles, France (Vol. **2125**, p. 16).

Das, I. and Zoback, M.D., 2012. Microearthquakes associated with long period, long duration seismic events during stimulation of a shale gas reservoir. In *SEG Technical Program Expanded Abstracts 2012* (pp. 1-5). Society of Exploration Geophysicists.

Economides, M. J., Notle, K. G. 2000. Schlumberger Reservoir Simulation, 3rd Edition, pp. 5-8 to 5-21.

Engelder, T. and Lash, G.G., 2008. Marcellus Shale Play" s Vast Resource Potential Creating Stir in Appalachia.

Ettensohn, F.R., 1985. The Catskill delta complex and the Acadian orogeny: A model. Geological Society of America Special Papers, 201, pp.39-50.

Ettensohn, F.R., Miller, M.L., Dillman, S.B., Elam, T.D., Geller, K.L., Swager, D.R., Markowitz, G., Woock, R.D. and Barron, L.S., 1988. Characterization and implications of the Devonian-Mississippian black shale sequence, eastern and central Kentucky, USA: Pycnoclines, transgression, regression, and tectonism.

Farnbach, J.S., 1975. The complex envelope in seismic signal analysis. *Bulletin of the Seismological Society of America*, **65**(4), pp.951-962.

Glasbergen, G., Yeager, V.J., Reyes, R.P. and Everett, D.M., 2010. Fluid-diversion monitoring: the key to treatment optimization. *SPE Production & Operations*, **25**(03), pp.262-274.

Ha, S.T.T., Sheriff, R.E. and Gardner, G.H.F., 1991. Instantaneous frequency, spectral centroid, and even wavelets. *Geophysical Research Letters*, **18**(8), pp.1389-1392.

Hardage, B., 2010. GC Instantaneous Seismic Attributes Calculated by the Hilbert Transform. Search and Discovery Article #40564.

Holley, E. and Kalia, N., 2015. Fiber-optic Monitoring: Stimulation Results from Unconventional Reservoirs. Unconventional Resources Technology Conference (URTEC).

Kallweit, R.S. and Wood, L.C., 1982. The limits of resolution of zero-phase wavelets. *Geophysics*, **47**(7), pp.1035-1046.

Karaman, O.S., Kutlik, R.L. and Kluth, E.L., 1996, January. A field trial to test fiber optic sensors for downhole temperature and pressure measurements, West Coalinga Field, California. In *SPE Western Regional Meeting*. *Society of Petroleum Engineers*.

Kavousi, P., Carr, T., Wilson, T., Amini, S., Wilson, C., Thomas, M., MacPhail, K., Crandall, D., Carney, B.J., Costello, I. and Hewitt, J., 2017. Correlating distributed acoustic sensing (DAS) to natural fracture intensity for the Marcellus Shale. In *SEG Technical Program Expanded Abstracts 2017* (pp. 5386-5390). Society of Exploration Geophysicists.

Kimbell, J., 2013. *History and Analysis of Distributed Acoustic Sensing (DAS) for Oilfield Applications* (Doctoral dissertation).

Kugler, I., Olmstead, R. 2015. North America Supply Analytics: Pennsylvania Marcellus.

Kumar, A., Zorn, E., Hammack, R. and Harbert, W., 2016. Surface Seismic Monitoring of Hydraulic Fracturing Activity in Pennsylvania and West Virginia. Unconventional Resources Technology Conference (URTEC).

Lash, G.G. and Engelder, T., 2011. Thickness trends and sequence stratigraphy of the Middle Devonian Marcellus Formation, Appalachian Basin: Implications for Acadian foreland basin evolution. *AAPG bulletin*, **95**(1), pp.61-103.

Li, M., Wang, H. and Tao, G., 2015. Current and future applications of distributed acoustic sensing as a new reservoir geophysics tool. *Open Petroleum Engineering Journal*, **8**(1), pp.272-281.

MacPhail, W.F., Lisoway, B. and Banks, K., 2012, January. Fiber optic distributed acoustic sensing of multiple fractures in a horizontal well. In SPE Hydraulic Fracturing Technology Conference. *Society of Petroleum Engineers*.

Madsen, K.N., Thompson, M., Parker, T. and Finfer, D., 2013. A VSP field trial using distributed acoustic sensing in a producing well in the North Sea. *First Break*, **31**(11), pp.51-56.

Mateeva, A., Mestayer, J., Cox, B., Kiyashchenko, D., Wills, P., Lopez, J., Grandi, S., Hornman, K., Lumens, P., Franzen, A. and Hill, D., 2012. Advances in distributed acoustic sensing (DAS) for VSP. In SEG Technical Program Expanded Abstracts 2012 (pp. 1-5). Society of Exploration Geophysicists.

Mateeva, A., Mestayer, J., Yang, Z., Lopez, J., Wills, P., Roy, J. and Bown, T., 2013. Dual-well 3D VSP in deepwater made possible by DAS. In *SEG Technical Program Expanded Abstracts 2013* (pp. 5062-5066). Society of Exploration Geophysicists.

Mestayer, J., Cox, B., Wills, P., Kiyashchenko, D., Lopez, J., Costello, M., Bourne, S., Ugueto, G., Lupton, R., Solano, G. and Hill, D., 2011. Field trials of distributed acoustic sensing for geophysical monitoring. In *SEG Technical Program Expanded Abstracts 2011* (pp. 4253-4257). Society of Exploration Geophysicists.

Miller, D., Parker, T., Kashikar, S., Todorov, M. and Bostick, T., 2012. Vertical seismic profiling using a fiber-optic cable as a distributed acoustic sensor: 74th EAGE Conference and Exhibition. In *Expanded Abstracts*.

Milliken, K.L., Rudnicki, M., Awwiller, D.N. and Zhang, T., 2013. Organic matter–hosted pore system, Marcellus formation (Devonian), Pennsylvania. *AAPG bulletin*, **97**(2), pp.177-200.

Molenaar, M.M. and Cox, B.E., 2013, January. Field cases of hydraulic fracture stimulation diagnostics using fiber optic distributed acoustic sensing (DAS) measurements and Analyses. In SPE Unconventional Gas Conference and Exhibition. *Society of Petroleum Engineers*.

Molenaar, M.M., Hill, D., Webster, P., Fidan, E. and Birch, B., 2012. First downhole application of distributed acoustic sensing for hydraulic-fracturing monitoring and diagnostics. *SPE Drilling & Completion*, **27**(01), pp.32-38.

OpendTect Documentaion at: http://doc.opendtect.org/5.0.0/doc/od_userdoc/content/app_a/freq.htm

Parker, T., Shatalin, S. and Farhadiroushan, M., 2014. Distributed Acoustic Sensing–a new tool for seismic applications. *First Break*, **32**(2), pp.61-69.

Rahman, M., Zannitto, P.J., Reed, D.A. and Allan, M.E., 2011, January. Application of fiber-optic distributed temperature sensing technology for monitoring injection profile in Belridge field, diatomite reservoir. In SPE Digital Energy Conference and Exhibition. *Society of Petroleum Engineers*.

Rao, M. and Qiu, H., 1993. Process Control Engineering: A Textbook for Chemical, Mechanical, and Electrical Engineering, Vol. **1**. *Gordon and Breach Science, New York, NY, USA*.

Robertson, J.D. and Nogami, H.H., 1984. Complex seismic trace analysis of thin beds. *Geophysics*, **49**(4), pp.344-352.

Robertson, J.D. and Fisher, D.A., 1988. Complex seismic trace attributes. *The Leading Edge*, **7**(6), pp.22-26.

Shelley, R., Nejad, A., Guliyev, N., Raleigh, M., & Matz, D. (2014, October 21). Understanding Multi-Fractured Horizontal Marcellus Completions. *Society of Petroleum Engineers*. doi: 10.2118/171003-MS

Sheriff, R.E. and Geldart, L.P., 1995. *Exploration seismology*. Cambridge university press.

Sheriff, R.E., Taner, M.T., Koehler, F. and Frye, D., 1977. Extraction and interpretation of the complex seismic trace.

Sierra, J.R., Kaura, J.D., Gualtieri, D., Glasbergen, G., Sarker, D. and Johnson, D., 2008, January. DTS monitoring of hydraulic fracturing: experiences and lessons learned. In SPE Annual Technical Conference and Exhibition. *Society of Petroleum Engineers*.

Song, L., Paronish, T., Agrawal, V., Hupp, B., Sharma, S. and Carr, T.R., 2017. Depositional Environment and Impact on Pore Structure and Gas Storage Potential of Middle Devonian Organic Rich Shale, Northeastern West Virginia, Appalachian Basin. Unconventional Resources Technology Conference (URTEC).

Tai, S., 2009. *Analysis of frequency characteristics of seismic reflections with attenuation in thin layer zone: Methods and applications*. University of Houston.

Taner, M.T. and Sheriff, R.E., 1977. Application of amplitude, frequency, and other attributes to stratigraphic and hydrocarbon determination: section 2. Application of seismic reflection configuration to stratigraphic interpretation.

Taner, M.T., Koehler, F. and Sheriff, R.E., 1979. Complex seismic trace analysis. *Geophysics*, **44**(6), pp.1041-1063.

Tanimola, F. and Hill, D., 2009. Distributed fibre optic sensors for pipeline protection. *Journal of Natural Gas Science and Engineering*, **1**(4), pp.134-143.

Walker, K. J., Wutherich, K., Terry, I., Shreves, J. E., & Caplan, J. (2012, January 1). Improving Production in the Marcellus Shale Using an Engineered Completion Design: A Case Study. *Society of Petroleum Engineers*. doi: 10.2118/159666-MS.

Wang, G. and Carr, T.R., 2013. Organic-rich Marcellus Shale lithofacies modeling and distribution pattern analysis in the Appalachian Basin. *AAPG bulletin*, **97**(12), pp.2173-2205.

Webster, P., Wall, J., Perkins, C. and Molenaar, M., 2013. Micro-Seismic detection using distributed acoustic sensing. In *SEG Technical Program Expanded Abstracts 2013* (pp. 2459-2463). Society of Exploration Geophysicists.

White, R.E., 1991. Properties of instantaneous seismic attributes. *The Leading Edge*, **10**(7), pp.26-32.

Widess, M.B., 1982. Quantifying resolving power of seismic systems. *Geophysics*, **47**(8), pp.1160-1173.

Wilson, T., Carr, T., Carney, B.J., Hewitt, J., Costello, I., Jordon, E., MacPhail, K., Uschner, N., Thomas, M., Akin, S. and Magbagbeola, O., 2016. Microseismic and model stimulation of natural fracture networks in the Marcellus Shale, West Virginia. In *SEG Technical Program Expanded Abstracts 2016* (pp. 3088-3092). Society of Exploration Geophysicists.

Yilmaz, O., 1987. Seismic Data Processing: Society of Exploration Geophysicists.

Zagorski, W.A., Wrightstone, G.R. and Bowman, D.C., 2012. The Appalachian Basin Marcellus gas play: Its history of development, geologic controls on production, and future potential as a world-class reservoir.

Zhang, J.J. and Bentley, L.R., 2000. Complex seismic trace analysis and its application to time-lapse seismic surveys. *CREWES, Geology and Geophysics, University of Calgary*.